Chemical Engineering Journal 173 (2011) 813–827

Contents lists available at ScienceDirect

Chemical Engineering Journal

journal homepage: www.elsevier.com/locate/cej

Assessment of mass transfer in the stagnant liquid regions in trickle-bed reactors

Clarisa Mocciaro[a,*], Osvaldo M. Martínez[a,b], Guillermo F. Barreto[a,b]

[a] PROIRQ, Departamento de Ingeniería Química, Facultad de Ingeniería, UNLP, La Plata, Argentina
[b] Centro de Investigación y Desarrollo en Ciencias Aplicadas "Dr. J. J. Ronco" (CINDECA) CONICET - UNLP - CCT La Plata, calle 47 No. 257, CP B1900AJK, Argentina

ARTICLE INFO

Article history:
Received 16 December 2010
Received in revised form 9 August 2011
Accepted 11 August 2011

Keywords:
Mass transfer
Trickle-bed reactors
Stagnant hold-up

ABSTRACT

A critical revision has been carried out of experimental investigations to quantify the size of the liquid stagnant region in fixed beds with co-current gas–liquid down-flow, and its ability to exchange mass with the dynamic region and with the particle surface. The revision has exposed that a high level of uncertainty arise to estimate, particularly, the mass exchange rate from the available evidence. Therefore, a second purpose is to introduce a geometric model to represent the stagnant region for spherical particles from which, assuming that diffusion is the only mass transport mechanism, it becomes possible to estimate the mass exchange rates with the dynamic region and with the particle surface. Finally, it was discussed why to expect that the geometric model is able to provide a lower bound to mass exchange rate with the dynamic region and a tight lower bound to mass exchange rate with the catalyst surface.

1. Introduction

Catalytic gas–liquid reactors, in particular fixed bed reactors with co-current downflow, known as trickle bed reactors (TBR), have been commonly employed in petroleum refining and petrochemistry. Of special importance is the kind of hydrotreatment processes (hydrodesulfurization, hydrorefining, hydrodenitrification, hydrocracking, etc.), as described, *e.g.* by Martínez et al. [1] and Furimsky [2], hydrogenation reactions [3,4], catalytic oxidations [5] and hydrocarbon synthesis by the Fischer–Tropsch process [6]. The above traditional applications of TBRs have been extended into new fields as biochemical, electrochemical and waste-treatment processes [7]. An important example is the use of biofilters to eliminate harmful organic compounds either from gaseous (typically air), *e.g.* Smith et al. [8], or liquid (typically water), *e.g.* Fortuny et al. [9], Horowitz et al. [10].

Promoted by the wide range of applications, conceptual and practical aspects of TBRs have been intensively studied over the last four decades. Several relevant revisions on the subject can be found in the literature: Mederos et al. [11], Biardi and Baldi [3], Dudukovic et al. [7], Al Dahhan et al. [12], Saroha and Nigam [13], Gianetto and Specchia [14], and Zhukova et al. [15].

In order to simulate mathematically the behavior of a TBR, apart from a proper kinetic knowledge of the catalytic reactions involved, it is essential to describe the flow of the gas and liquid phases at the global scale of the bed and at the local scale of the catalytic particles. The last issue should allow quantifying the rate of mass and energy exchange between the fluids and the catalyst [1,7,13].

In this sense, it is well known that the contact of the external surface of the catalyst particles with the fluids is not uniform, as part of that surface will be in direct contact with the gas phase (dry area) and the remaining part with the liquid phase (wetted area). The extent of the dry area is strongly dependent of the superficial liquid velocity. In turn, the local field of liquid velocities around the wetted area is not uniform either. In some studies [16,17] the distribution of liquid flow is described in terms of its "morphology" or "texture". A clear picture showing the features of the liquid irrigation over the packing has been provided by the use of Magnetic Resonance Imaging, as reported by Sankey et al. [18]. While this kind of studies can provide a great deal of details about the liquid flow characteristics, apparently there is not a procedure developed at present to turn the information gained into a framework for predicting mass and heat transfer rates to the catalyst surface, in the context of conventional models to simulate TBRs.

Therefore, as regards specifically the evaluation of mass transfer from the flowing liquid to the external particle surfaces, two main approaches have been employed in most studies. In the first approach, the non-uniformities of the wetted surface are not explicitly accounted for, while the evaluation of the mass exchange rate between the liquid stream and the particle surface is carried out by relying upon a global mass transfer coefficient k_{Lp}, defined over the whole wetted-area. The extent of the latter is estimated from correlations of the so-called wetting efficiency f_w (the wetted fraction of the external particle surfaces), from which the specific wetted area a_w can be evaluated.

In the second approach, the effect of the non-uniform liquid flow around the packing surface, on the contrary, is explicitly

* Corresponding author. Tel.: +54 2214221913; fax: +54 2214254277.
E-mail address: clarisamocciaro@hotmail.com (C. Mocciaro).

1385-8947/$ – see front matter © 2011 Elsevier B.V. All rights reserved.
doi:10.1016/j.cej.2011.08.032

Nomenclature

a_d	particle surface wetted by the dynamic liquid per bed volume (m^2/m^3)
a_s	particle surface wetted by the stagnant liquid per bed volume (m^2/m^3)
a_w	wetted external particle surfaces per bed volume (m^2/m^3)
a_{ds}	area of boundary between stagnant and dynamic regions per bed volume (m^2/m^3)
A_d	portion of particle surface in contact with dynamic region (m^2)
A_{dry}	portion of dry particle surface (m^2)
A_p	particle surface (m^2)
A_s	portion of particle surface in contact with stagnant region (per contact point) (m^2)
Bi_{sp}	Biot number ($=k_{sp}d_p/(2D_{eff})$)
C	local molar concentration in the stagnant region (mol/m^3)
C_d	molar concentration in the dynamic region (mol/m^3)
C_s	average molar concentration in the stagnant region (mol/m^3)
C_{sp}	average molar concentration on A_s (mol/m^3)
D_{eff}	effective diffusivity (m^2/s)
$\mathcal{D}_m$	molecular diffusivity (m^2/s)
D_L	axial dispersion coefficient (m^2/s)
d_p	particle diameter (m)
f_d	fraction of particle surface wetted by the dynamic liquid
f_s	fraction of particle surface wetted by the stagnant liquid
f_w	fraction of wetted particle surface
H_d	dynamic liquid hold-up (dynamic liquid volume per bed volume)
H_r	residual liquid hold-up (residual liquid volume per bed volume)
H_s	stagnant liquid hold-up (stagnant liquid volume per bed volume)
H_t	total liquid hold-up (liquid volume per bed volume)
j_{ds}	average flux trough A_{ds} ($mol/(m^2\,s)$)
j_{sp}	average flux trough A_s ($mol/(m^2\,s)$)
k_{dp}	mass transfer coefficient between dynamic liquid and particle surface (m/s)
k_{ds}	mass transfer coefficient between dynamic and stagnant regions (m/s)
k_{Lp}	global mass transfer coefficient between liquid stream and wetted particle surface (m/s)
k_{sp}	mass transfer coefficient between stagnant regions and particle surface (m/s)
N_c	number of contact points per particle
R	homogeneous source term ($mol/(m^3 s)$)
Re_L	liquid Reynolds number ($=\rho_L u_L d_p/\mu_L$)
Sh^*	Sherwood number, Eq. (2)
Sh_{ds}	Sherwood number ($=k_{ds}d_p/\mathcal{D}_m$)
Sh_{dsp}	Sherwood number ($=d_p^2/(\Omega_{dsp}\,\mathcal{D}_m)$)
Sh^*_{Lp}	Sherwood number, Eq. (14)
Sh_{sp}	Sherwood number ($=k_{sp}d_p/\mathcal{D}_m$)
t	time (s)
u_G	superficial gas velocity (m/s)
u_L	superficial liquid velocity (m/s)
V_s	half volume of elementary stagnant region (m^3)
V_p	particle volume (m^3)
z	bed axial coordinate (m)
Z	bed height (m)

Greek letters

ε	bed void fraction
ε_P	particle porosity
φ	angle of elementary stagnant region (Fig. 1) (°)
μ_L	liquid viscosity (Pa s)
ρ_L	liquid density (kg/m^3)
τ	tortuosity factor
Ω_{dsp}	global mass transfer resistance ($=(a_s k_{sp})^{-1}+(a_{ds}k_{ds})^{-1}$) (s)

recognized. The volume of interstitial liquid contained in the bed is divided in a fraction with hold-up H_d, which flows with uniform velocity (dynamic region) and the remaining fraction with hold-up H_s, which does not participate of the liquid flow (stagnant region). Thus, the distribution of axial velocities is approximated by means of a sharp division. The stagnant region develops in the space around the contact points between the particles, where the large surface to volume ratio, due to interfacial forces, hinders the mobility of the liquid. This second approach is identified here as the two wetted zone (TWZ) model.

In simulating TBRs, the TWZ model is a conceptual advance over the non-discriminating first approach that can be expected to provide a more adjusted description of the interactions between diffusion-reaction process inside the particle and external mass transport. Hence, the TWZ model has been employed in several studies of TBR: Liu et al. [19], Nijhuis et al. [20], Eftaxias et al. [21], Chaudhari et al. [22], Iliuta and Larachi [23], Rajashekharam et al. [24]. However, the estimation made in those studies of the mass transport parameters defined for the TWZ model are, in general, questionable. The reasons for this assertion can be partially found in the inspection and analysis of the available experimental evidence about the mass transfer coefficients, especially those related to the stagnant region.

Then, a first goal of this contribution is to perform a critical revision of the experimental investigations carried out to quantify the size of the stagnant region and its ability to exchange mass with the dynamic region and with the particles. The revision reveals that a high level of uncertainty will arise to estimate, particularly, the mass exchange rate from the available evidence. Therefore, a second purpose is to introduce a geometric model to represent the stagnant region for spherical particles from which, assuming that diffusion is the only mass transport mechanism, it becomes possible to estimate the mass exchange rates with the dynamic region and with the particle surface. We will also discuss reasons to expect that the geometric model is able to provide a lower bound to mass exchange rate with the dynamic region and a tight lower bound to mass exchange rate with the catalyst surface.

2. Analysis of the literature background

The parameters introduced by the TWZ model can be visualized with the help of Fig. 1. The specific particle surface wetted by the dynamic and stagnant regions are identified by a_d and a_s, respectively ($a_w = a_d + a_s$). The dynamic region also maintains a hypothetical interface with the stagnant region extended over a specific surface area identified as a_{ds}. The external surface of each particle (see the inset in Fig. 1) becomes in this way divided in three parts: the stagnant zones (area $N_c A_s$), the dynamic zone (area A_d) and the dry area ($A_{dry} = A_p - N_c A_s - A_d$). In these relationships, N_c is the average number of contact points per particle (also known as coordination number). As regards mass exchange between the

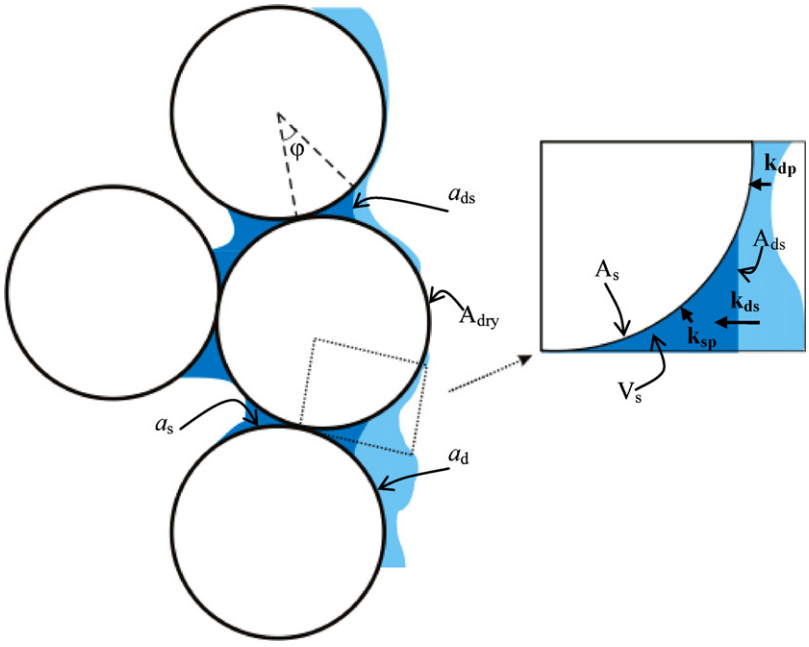

Fig. 1. Two wetted zone model (TWZ).

flowing liquid and the external particle surface, three mass transfer coefficients are introduced: k_{dp} between dynamic region and particle surface (across a_d), k_{sp} between stagnant region and particle surface (across a_s) and k_{ds} between dynamic and stagnant regions (across a_{ds}) (see the inset in Fig. 1).

In principle, geometrical and exchange properties of the stagnant region of the TWZ model can be assessed by employing and complementing results from a variety of experimental techniques. However, the literature survey indicates that experimental data expressly processed to characterize the stagnant region of the TWZ model are based on tracer-response techniques. Therefore, the following discussion will be focused on the results from the use of such techniques.

Characteristics of the packing and fluids, main operating conditions and the type of tracer techniques employed in the contributions discussed here are displayed in Table 1. The experiments were mostly performed on beds with co-current down-flow, although counter-current flow was studied in a couple of them, which were included in the present analysis for the sake of completeness. As regards the studies with co-current down-flow, most of the reported data correspond to gas and liquid superficial velocities corresponding to the trickling regime (low interaction regime), but some measures pertaining to the transition or pulsing regimes were occasionally included [25,26].

The list in Table 1 includes different particle shapes: spheres, cylinders, tablets, irregular particles (powder), extrudates and Rasching rings. Water and air were by far the common employed fluids. Mostly salts, analyzed by conductimetry, were employed as tracers.

The tracer was injected in the form of impulse-function or step-function, as reported in Table 1. As is well known, the response to the former is related to the residence time distribution (RTD) and the latter to the cumulative residence time distribution.

A relevant distinction to be made concerns the use of porous or non-porous packing. As regards transport parameters, the use of the latter in tracer-response experiments only allows to extract information about the dynamic/stagnant mass transfer coefficient, k_{ds}. Clearly, the transport from the stagnant zone to the catalyst surface of the packing, involving the coefficient k_{sp}, is not activated. On the contrary, for porous packing, the tracer will also be transferred from the stagnant region to the inside of the particles. However, in the study of Iliuta et al. [27] (see Table 1) the transport from the stagnant region towards the porous particles was lumped with that of the dynamic region. Therefore, only in the contributions of Iliuta et al. [28] and Nigam et al. [29] the coefficient k_{sp} was estimated from the analysis of the tracer-response experiments. These results for k_{sp} will be discussed in Section 4 and in the next section we will focus the information concerning the mass transfer coefficient k_{ds}.

A few works were devoted to characterize the stagnant regions in co-current up-flow, as those of Yang et al. [30] and Iliuta et al. [31] (not included in Table 1). In this system, the fluid dynamics is very different to the case of liquid down-flow. These studies will not be analyzed in the present contributions.

2.1. Models employed to analyze tracer-response experiments

As in all experimental contributions the tracer employed was a nonvolatile species, only the behavior of the liquid phase had to be modeled to interpret the response of the system to the perturbation made by the injection of the tracer. Either piston flow or axially dispersed piston flow were assumed for the global flow of the liquid through the bed. In either case, the transfer rate of the tracer from the liquid stream to the stagnant region and to the inside of the particles (when porous particles were employed) was added to the mass conservation expressions. Thus, broadly speaking, the models employed can be classified as piston-exchange (PE) model and piston-dispersion-exchange (PDE) model. Table 2 summarizes the use of PE or PDE models in the different studies.

As commented on above, the exchange of tracer between the stagnant region and the packing was not accounted in most cases; hence, in these cases the conservation mass balance for tracer in the stagnant zone reads:

$$H_s \frac{\partial C_s}{\partial t} = a_{ds} k_{ds} (C_d - C_s) \quad (1)$$

The common parameters in all experiments are the total liquid hold-up H_t, the stagnant liquid hold-up H_s and the volumetric mass exchange coefficient ($a_{ds}k_{ds}$). Additionally, the PDE model adds the mass dispersion coefficient D_L.

Table 1
Operating conditions and experimental techniques.

References	Packing	Particle shape	d_P (mm)	Process fluids	u_L (mm/s)	u_G (m/s)	Experimental method	Tracer
Iliuta et al. [27]	Porous	Sphere	3.3	Air/water	2.1–9.2	0.028–0.41	Impulse function	KCl
Iliuta et al. [27]	Non-porous	Sphere	3	Air/water	5–17	0.028–0.7	Impulse function	KCl
Iliuta et al. [28]	Porous	Sphere	3.3	Air/water	2.1–9.2	0.028–0.41	Impulse function	KCl
Nigam et al. [29]	Porous	Sphere/tablet/extrudate	3 (sphere)/7.62 (tablet)/5.14 (holed tablet)/3.4–4.5–7.2 (extrudate)	Air/water	4.6–18.3	0–27.4	Impulse function	Radioactive substance
Matsuura et al. [34]	Non-porous	Sphere	1.2–2.6–4.3	Air/water	2–100	0.02–0.2	Impulse function	KCl
Van Swaaij et al. [35]	Non-porous	Raschig ring	2.13–4.41–8.72	Air/water	2–10	–	Impulse function	NaCl
Sicardi et al. [40]	Non-porous	Ring	2.65	Air/water	0.55–7.29	0–0.61	Step function	KCl/$ZnSO_4$
Hochman and Effron [41]	Non-porous	Sphere	4.76	Nitrogen/methanol	1–10	≤0.085	Impulse function	KSCN
Tsamatsoulis and Papayannakos [42]	Non-porous	Powder/extrudate	0.4–3.35	Hydrogen/HVGOs	0.1–10	5.48×10^{-4}–3.2×10^{-2}	Step function	Sulphur
Stegeman et al. [46]	Non-porous	Sphere	3	Air/water//sol ETG	1–10	≤0.14	Impulse function	KBr
Bennett and Goodridge [25][a]	Non-porous	Raschig ring	8.45–16.2	Air/water	1.8–21	–	Step function	$ClNH_4$
Hoogendoorn and Lips [26][a]	Non-porous	Raschig ring	16.2	Air/water	1.52–5.18	13.71–51.81	Impulse function	$ClNH_4$

ETG: ethylene glycol; HVGO, Heavy Vacuum Gas Oil.
[a] Counter-currently.

Table 2
Models and regression criteria used in the studies listed in Table 1.

Reference	Model	Regression criterion
Iliuta et al. [27] (porous)	PDE and intraparticle diffusion	MinObjFun.
Iliuta et al. [27] (non-porous)	PDE	MinObjFun.
Iliuta et al. [28]	PDE and intraparticle diffusion	MinObjFun
Nigam et al. [29]	PDE and intraparticle diffusion	MinObjFun
Matsuura et al. [34]	PDE	Method of moments/MinObjFun
Van Swaaij et al. [35]	PDE	Method of moments
Sicardi et al. [40]	PE/PDE	Method of moments/MinObjFun/Bennett and Goodridge's approach
Hochman and Effron [41]	PE	Method of moments/H_d graphically
Tsamatsoulis and Papayannakos [42]	PE	MinObjFun/H_d graphically
Stegeman et al. [46]	PDE	Method of moments/MinObjFun
Bennett and Goodridge [25]	PDE	Method of moments and graphical method
Hoogendoorn and Lips [26]	PE	Method of moments/H_d graphically

MinObjFun, Minimization of an objective function based on the differences between theoretical and experimental tracer-response curves.

When porous particles are employed, the conservation balance in the particles should be added to the formulation. As the existence of the stagnant zone is recognized, non-uniform boundary conditions would have to be considered in order to distinguish the different rates of mass exchange through the dynamic, stagnant and, eventually, dry zones of the external surface. However, this effect was not considered in none of the works with porous particles and the conservation balances were formulated under the assumption of spherical symmetry. The effective diffusivity of the tracer inside the particles D_{eff} is introduced as an extra parameter. Eventually, some other parameters might have to be considered if adsorption of the tracer turns out to be significant [32]. As regards external mass transfer towards the inside of porous particles, the volumetric mass transfer coefficients ($a_d k_{dp}$), from the dynamic region, and ($a_s k_{sp}$), from the stagnant region, would have to be included.

It is evident that the system includes a large number of parameters, particularly if porous particles are used. In the studies listed in Table 1 many different approaches have been employed to reduce the number of parameters that were fitted to the response of tracer injection, mainly by estimating some of them from existing information from the bibliography, from complementary experiments or making simplifying assumptions.

2.2. Regression criteria

Three different criteria have been mainly employed to fit the parameters of the models to the tracer injection experiments: the method of moments (see, *e.g.* Chapter 5 in ref. [33]), minimization of an objective function based on the differences between theoretical and experimental tracer–response curves and graphical comparison of experimental with theoretical responses.

Some *ad hoc* criteria have also been used. For instance, in some studies the dynamic hold-up H_d was evaluated by identifying the earliest appearance of the tracer in the response curve to a pulse or step-function injection. The stagnant liquid hold-up H_s is then estimated by subtracting H_d to the total hold-up H_t associated to the first moment of the RTD.

Another specific and more elaborated procedure was developed by Bennett and Goodridge [25], who used non-porous particles. They identified two straight segments on a plot of the logarithm of the tracer concentration at the bed outlet vs. the time elapsed from the pulse injection. Their analysis indicated that the slope of the first straight segment is strongly related to the magnitude of the axial dispersion coefficient D_L and shows little effect of the stagnant regions. At this time, the stagnant regions retain part of the injected tracer from the liquid stream. In the transition part of the response, between the two straight segments, the flux of the tracer exchanged between dynamic and stagnant regions changes direction. Thus, according to the authors, the amount of tracer detected in the second straight segment is just released from the stagnant regions (*i.e.* if the stagnant regions were absent, the second straight segment would not be recorded). Quantitatively, the slope of the second straight segment corresponds to $a_{ds}k_{ds}$. Furthermore, the analysis of the authors allowed them to estimate the ratio H_d/H_t from the ordinate intercept of the second straight segment.

Table 2 shows a summary of the different tracer–response models including the criteria for the parameter estimation.

2.3. Discussion of the results from the experimental studies

It is first convenient to discuss the general behavior of the experimental RTDs. In all cases, the RTDs show considerable long tails, a fact clearly indicating a significant amount of liquid elements that expend times in the bed of up to an order of magnitude longer than the mean residence time.

The strong asymmetry of the RTD produced by the long tails is a clear evidence of the existence of liquid pockets inside the bed with negligible mobility, which can be regarded to built up the stagnant regions [33]. In fact, several authors [26,34–37] reported that the measured RTDs failed to be correctly fitted to the conventional axial dispersion model (without considering the stagnant regions) because of the tails of the experimental curves.

In this section, we will discuss the results from the sources in Table 1 and for two of the parameters concerning the stagnant region: $a_{ds}k_{ds}$ and H_s.

2.3.1. Experimental results for the volumetric coefficient $a_{ds}k_{ds}$

It has been found convenient, in order to systemize the results of $a_{ds}k_{ds}$ from different sources, to introduce the modified Sherwood number defined as:

$$Sh^* = \frac{a_{ds}k_{ds}d_P^2}{(1-\varepsilon)\mathcal{D}_m}, \quad (2)$$

where for the non-spherical particles d_p is the diameter of a sphere with the same ratio surface to volume as the particle.

The experimental values of Sh^* are plotted in Fig. 2 as a function of the liquid Reynolds number Re_L. Symbols correspond to data points and continuous lines to some correlations developed from experimental results, except the horizontal lines identified as Sh^*_{min} and Sh^*_{max} and the curve labeled Sh^*_{Lp}, which will be explained later on.

The most striking feature from Fig. 2 is the huge dispersion among the data from the different sources, spanning about two orders of magnitude.

We believe that there are several reasons that contribute to such degree of dispersion. A first and conceptual point is the fact that there is no a real interface between the dynamic and stagnant regions. Instead, the TWZ model quantifies mass exchange relying

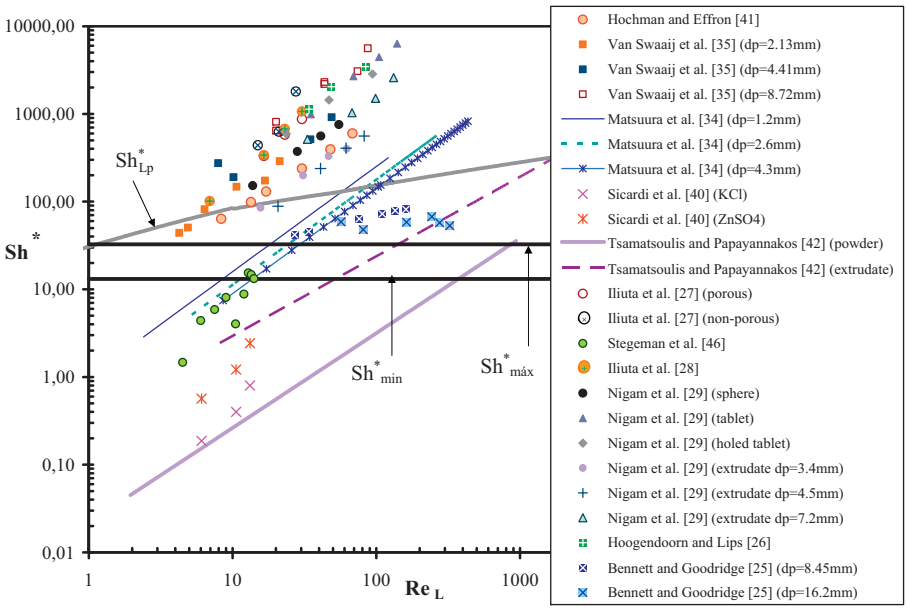

Fig. 2. Values of Sh^* [Eq. (2)] reported in the studies listed in Table 1 vs. Re_L.

upon a "mass transfer coefficient concept", which is proper of a true interface.

Also, it is well known that the experimental evaluation of any effective fluid dynamic property in trickle beds is subject to a strong level of uncertainty, a problem in large part related to the fluctuations of the liquid flow. Besides, the liquid flow pattern is not a unique function of the operating conditions, depending upon the operation story. For instance, it is acknowledged that significant differences in fluid dynamic behavior are found whether the bed was previously flooded, or not, before setting up the stationary operating conditions [38].

Some points, owing to the response–tracer technique, can be quoted as contributions to the dispersion in Fig. 2. First, it is recalled that even when the effect of the stagnant regions is clearly identifiable by the presence of long tails in the RTD, the procedures to obtain quantitative information characterizing the stagnant region may not provide reliable results. This is due to the lost of precision in measuring the tracer concentration at the low level in the tails and, in addition, to the natural fluctuations that are characteristic of the liquid-flow in trickle beds [39]. The difficulties in the treatment of the RTD tail becomes clear, for example, in the study of Hoogendoorn and Lips [26], who stopped the record of the response when the tracer was still being eluted. To gain an insight into how the correct assessment of the RTD tails affect the estimation of the stagnant region parameters we write the stagnant region contributions to the first and second order centered moments, $\Delta\bar{t}$ and $\Delta\sigma$, respectively (*e.g.* Sicardi et al. [40]; Hochman and Effron [41]; Hoogendoorn and Lips [26]):

$$\Delta\bar{t} = H_s \frac{Z}{u_L} \tag{3a}$$

$$\Delta\sigma^2 = 2H_s^2 \frac{Z}{u_L} \frac{1}{a_{ds}k_{ds}} \tag{3b}$$

If the moments are not directly used as a fitting criterion, the relevance of them will be in someway reflected in any of the method employed to adjust the parameters (Section 2.2).

It becomes clear from Eq. (3a) that the estimation of H_s is directly affected by the precision of the measures of $\Delta\bar{t}$. The quality of estimation of $a_{ds}k_{ds}$ is directly related to the precision of the measures of $\Delta\sigma^2$, but in addition it is also critically affected by the values of H_s, because of its quadratic dependence. As discussed below, in some studies H_s was not estimated from the tracer–response, but it was evaluated from independent correlations, a fact likely to introduce important deviations on the estimation of $a_{ds}k_{ds}$.

The choice of the model to analyze the response can also be a source of data dispersion in Fig. 2. For example, the use of the PE model implies that the whole dispersion of the RTD will be attributed to the effect of the stagnant regions, as the intrinsic axial dispersion is ignored. Thus, for the results of the studies reported in [26,41,42] employing the PE model, the effect of the stagnant regions could has been overemphasized.

Sicardi et al. [40] discussed the effect of the regression criteria. They employed the three main procedures mentioned at the beginning of Section 2.2 to the same experimental data, and found significant deviations in the fitting values of the parameters, reaching in some instances a factor of 5.

It was already mentioned (Section 2.1) that a significant number of parameters arise when using porous particles. Realizing that is practically impossible to estimate all of them from tracer–response experiments, some were independently evaluated in the contributions listed in Tables 1 and 2. The mass transfer coefficient from the dynamic region to the particle surface (k_{dp}) was in all studies estimated from existing correlations of the global mass transfer coefficient k_{Lp} between the liquid stream and the particle surface. Apart from the fact that correlations of k_{Lp} are normally based on steady state measurements (at variance with the transient phenomena in tracer–response experiments) and include contributions through both, dynamic and stagnant regions, such correlations are subject to some degree of uncertainty [38]. Any deviation from the right value of k_{Lp} is most likely to affect the fitted value of k_{ds}, as both transfer processes, towards the inside of the particles and towards the stagnant regions, contribute to the dispersion of the RTD. The effective diffusion coefficient D_{eff} inside the particles has also been evaluated independently and again is likely to add uncertainty, because of the same reasons, to the estimation of k_{ds}. In addition, in those studies that specifically include the estimation of mass transfer between the stagnant regions and particles, k_{sp}, [28,29], the stagnant liquid hold-up H_s was estimated from the Saenz and Carbonell [43] correlation for the so-called residual liquid hold-up (H_r). This is the amount of liquid retained in the bed after a sudden termination of the liquid fed to the bed. We will come back later to the discussion of H_r in Section 2.3.2, but it should be

said here that although H_s and H_r are related, there is an experimentally observed trend for H_r to be larger than H_s. The effect of an uncertain estimation of H_s on $a_{ds}k_{ds}$ has already been discussed in relation to Eq. (3b).

In Fig. 2, the data for all particle shapes are included. If only the data for spherical are considered, the data dispersion continues to be very high for them. Seemingly, the group of non-spherical shapes (mainly cylindrical particles) nearly keeps the same degree of dispersion of the whole set of data.

Given the large dispersion of the experimental data, it is most important to explore the possibility to reduce the range of uncertainty, discarding or classifying as highly unreliable those data points showing very high or very low levels of Sh^*.

To this end, it will be presented in Section 3 a realistic geometrical description of an elementary stagnant region, based on its building up around a contact point, as illustrated in the inset of Fig. 1. If the stagnant regions are considered motionless, molecular diffusion will be the only transport mechanism inside them. Under this assumption, values of Sh^* for non-porous particles, as would arise from tracer-response experiments, are evaluated in Section 3.1. In that section, we will also explain the meaning of Sh^*_{min}, Sh^*_{max} and Sh^*_{Lp} plotted in Fig. 2.

2.3.2. Experimental results for the stagnant liquid hold-up H_s

The values of H_s used in the studies listed in Table 1 have been represented in the bar diagram of Fig. 3. Different values from the same source correspond to differences in the kind of particles used.

In most studies, values of the residual liquid hold-up H_r were either measured or estimated from existing correlations. These values are also included in Fig. 3 for each study. In general, the same value of H_r and H_s in Fig. 3 means that H_s was not experimentally evaluated and assumed equal to H_r, for estimating other parameters (*e.g.* $a_{ds}k_{ds}$), with the exception of the works of Hochman and Effron [41] and Hoogendoorm and Lips [26]. In these studies, H_r was measured and H_s evaluated from the RTD curves, and no significant differences were found between them. In the work of Sicardi et al. [40] a moderate effect of the superficial liquid velocity on H_s was found. The average value is plotted in Fig. 3. Also, the averages from different replicas reported by Iliuta et al. [27] are plotted.

The purpose of the assumption $H_s = H_r$ in several contributions was to reduce the number of fitting parameters in the analysis of tracer–response experiments. Nonetheless, taking $H_s = H_r$ may involve a biased estimation for H_s, as in many studies in which both were evaluated, H_s turned out to be significantly lower than H_r (see Fig. 3). This result admits a clear physical explanation. The residual liquid at non-flowing conditions is held around the contact points by the action of superficial forces exerted by the particle surface; also, patches of liquids formed by bridging of neighboring regions have been observed [45]. Once the flow of liquid is established, the areas around the contact-points are the preferred path for the liquid to flow from a piece of packing to the next below. Thus, apart from the superficial forces, the liquid around the contact points undergoes an additional dragging action and, as a result, a smaller amount will be retained [25,34,40,46,47].

As regards the effects of the fluid superficial velocities on H_s, u_G was found in most of the works to have essentially no influence and a marginal increasing trend of H_s with u_L was reported only in the works of Tsamatsoulis and Papayannakos [42], and Sicardi et al. [40]. Therefore, the values of H_s provided by Fig. 3 can be regarded as holding irrespective of u_G and u_L, according to the conclusions reached in the different studies.

A specific comment should be made about the very high values informed by Tsamatsoulis and Papayannakos [42]. The authors estimated H_d from the first appearance of the tracer in the RTD curves, a criterion consistent with their analysis based on the PE model (Table 2), and $H_t = H_d + H_s$ by matching the theoretical and experimental curves. It is likely that the value of H_d were underestimated, as the first appearance of the tracer may be caused by the intrinsic axial dispersion and not by the liquid front reaching the bed outlet. If so, H_s evaluated as $H_s = H_t - H_d$ will be overestimated, an effect that probably accounts for the comparatively large values of H_s in Fig. 3.

On the other hand, the values from Sicardi et al. [40] and one of the reported by Bennet and Goodridge [25] seem to be well below the average in Fig. 3. With the purpose of identifying a reliable range for values of H_s, the high values of Tsamatsoulis and Papayannakos [42] and two lowest values just mentioned can be disregarded. In this way, the following range covers the majority of data in Fig. 3:

$$0.01 < H_s < 0.06 \quad (4)$$

The range of probable values for the parameter H_s is thus much tighter than the range of experimental values of the transfer parameter $k_{ds}a_{ds}$ discussed in Section 2.3.1.

3. Geometric model for the stagnant regions

It is evident from the analysis made in Section 2 that the available experimental evidence does not allow to estimate with a reasonable degree of certainty the transport coefficient $a_{ds}k_{ds}$ that partially characterize the behavior of the stagnant region. Based on a more limited body of results, it will be shown that a similar conclusion arises for the second transport coefficient pertaining to

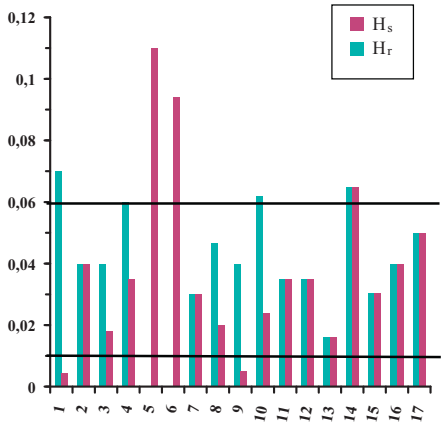

1 Sicardi *et al.* [40]
2 Hoogendoorm and Lips [26]
3 Matsuura *et al.* [34] dp=2.6mm
4 Matsuura *et al.* [34] dp=4.3mm
5 Tsamatsulis and Papayannakos [42] dp=0.4mm
6 Tsamatsulis and Papayannakos . [42] dp=2.35mm
7 Hochman and Effron [41]
8 Stegeman *et al.* [46]
9 Bennet and Goodridge [25] dp=8.45mm
10 Bennet and Goodridge [25] dp=16.2mm
11 Van Swaaij *et al.* [35] dp=2.13mm
12 Van Swaaij *et al.* [35] dp=4.41mm
13 Van Swaaij *et al.* [35] dp=8.72mm
14 Iliuta *et al.* [28]
15 Iliuta *et al.* [27] dp=3.3mm porous
16 Iliuta *et al.* [27] dp=3mm non-porous
17 Nigam *et al.* [29] sphere dp=3mm

Fig. 3. Values of stagnant liquid hold-up (H_s) and residual liquid hold-up (H_r) used in the studies listed in Table 1.

the stagnant region, $a_s k_{sp}$ (see Section 4). Although some shortcomings have been discussed in Section 2.3.1 about the treatment of the experimental data, we believe that the fundamental problem to measure reliable transport parameters stems in the fact that the stagnant region is an idealized description of a complex fluid-dynamic behavior around the contact points of the packing. Taking this view for granted, it is difficult to envisage alternative experimental procedures, replacing the tracer-response technique, to obtain significantly better results.

We recall here that the most relevant purpose for characterizing the stagnant region is the evaluation of its impact on the behavior of catalytic trickle bed reactors. Within this frame, an alternative to the lack of reliable experimental information is to develop a model capable to provide a reasonable lower limit to mass transfer rates along the stagnant regions. Thus, it can be expected that the real behavior of a trickle bed reactor can be bounded by the results from ignoring the existence of the stagnant region (*i.e.* employing global mass transfer coefficients) and from using the TWZ model with the stagnant zone parameters evaluated with the aid of such a model.

Therefore, in this section we will present a model for the stagnant regions in beds of spherical particles, termed Geometric Model, which is defined by two basic features. On one hand, an elementary stagnant region is assumed to fill the volume ($2\,V_s$) between the external surfaces of two contacting particles and a circular cylinder with axis coincident with the line joining both particle centers (inset in Fig. 1). The second feature is the assumption that mass transport inside the stagnant region just takes place by molecular diffusion. The only parameter introduced in the model is the half-volume V_s of the elementary stagnant region. If a reasonable value of V_s is chosen [*e.g.* leading to a value of H_s within the range in Eq. (4)], it can be expected that mass transfer rates evaluated from the model will be lower than the actual ones, as the liquid inside is assumed to show no mobility.

It should be noted that the proposed shape of the stagnant regions was already suggested by Sicardi et al. [48]. Similar approach was also taken by Ortiz-Arroyo et al. [49] and Mao et al. [50] to represent the residual liquid regions after interrupting the liquid flow (in this case, however, an indented lateral shape, caused by the effect of surface tension, is observed). As already mentioned, it has been observed that the residual liquid around neighboring contact point may form more extended liquid patches [45], although this is not pertinent under flowing operation. The assumed shape of the liquid region around contact-points (inset in Fig. 1) is frequently referred to as pendular ring.

The relationship between V_s and H_s can be written as:

$$\frac{V_s N_c (1-\varepsilon)}{V_p} = H_s \tag{5}$$

where $V_p = \pi d_p^3/6$ and N_c is the average number of contact points (coordination number) per particle.

For random beds of spheres ε depends on the ratio vessel diameter/particle diameter, but for the usual case of adiabatic trickle bed reactors this ratio is very large and ε can be reliably estimated as $\varepsilon = 0.37$–0.40. From the studies of Reimann et al. [51] and Salvat et al. [52], the average coordination number is around 6. The value $N_c = 6$ was adopted for the numerical results provided here.

Once V_s is estimated from (5), the elementary stagnant region becomes geometrically defined. Of particular importance are the particle surface area in contact with the stagnant region A_s (see the inset in Fig. 1) and the half–cylindrical area A_{ds} that connects the elementary stagnant region with the dynamic region (see the inset in Fig. 1). These can be better written in terms of the angle φ subtending the volume V_s (see Fig. 1):

$$V_s = \pi \frac{d_p^3}{24}(1-\cos\varphi)^2(1+2\cos\varphi) \tag{6}$$

In this way, φ can be alternatively regarded as the only parameter of the geometric model.Then,

$$A_s = \pi \frac{d_p^2}{2}(1-\cos\varphi) \qquad A_{ds} = (\sin\varphi)A_s \tag{7}$$

The specific areas a_s and a_{ds} can be readily evaluated:

$$a_s = \frac{3(1-\varepsilon)}{d_p} N_c (1-\cos\varphi); \qquad a_{ds} = (\sin\varphi)a_s \tag{8}$$

3.1. Use of the Geometric Model to evaluate the coefficient ($a_{ds}k_{ds}$) arising in tracer–response experiments with non-porous particles

In this section we will evaluate by means of the geometric model the coefficient $a_{ds}k_{ds}$, as it would arise from the tracer–response experiments with non-porous particles. The purpose is to compare the results with the experimental data in Fig. 2.

Considering that the tracer diffuses inside the idealized elementary stagnant region according to the Fick low with constant diffusion coefficient $\mathcal{D}_m$ a conservation balance for the tracer in V_s can be written

$$\frac{\partial C}{\partial t} = \mathcal{D}_m \nabla^2 C, \quad \text{in } V_s \tag{9a}$$

At the particle boundary:

$$\nabla C \cdot \mathbf{n} = 0, \quad \text{at } A_s \tag{9b}$$

In (9b), $\mathbf{n}$ is the local unit vector normal to A_s. As regards the interface with the dynamic region, we will assume here that the resistance in the dynamic zone can be neglected with respect to that in the stagnant region. Then,

$$C = C_d, \quad \text{at } A_{ds} \tag{9c}$$

where C_d can be regarded as being uniform on A_{ds}.

It is noted that C_d and C will depend on the time t elapsed from the injection of the tracer and on the bed axial coordinate z. In addition, C depends on the local coordinates describing V_s and its boundaries. Initial conditions for (9a) will be $C = 0$.

The mass transfer coefficient k_{ds} is, in general, defined from:

$$k_{ds}(C_d - C_s) = j_{ds} = \frac{\mathcal{D}_m \int_{A_{ds}} (\nabla C \cdot \mathbf{n})\, dA}{A_{ds}} \tag{10a}$$

where j_{ds} is the average flux of tracer incoming to the stagnant region (trough A_{ds}), $\mathbf{n}$ is the unit vector normal to an element dA of A_{ds} oriented outside the stagnant region and the average tracer concentration C_s is given by:

$$C_s = \frac{\int_{V_s} C\, dV}{V_s} \tag{10b}$$

It becomes clear from Eq. (10a) that k_{ds} is a function of t and z, for C satisfying the problem (9a)–(9c). This feature is due to the fact that in the present approach the stagnant region is described by a distributed model (Geometric Model), at variance with the lumped model employed to analyze the experimental information (Eq. (1)). Therefore, an RTD using the Geometric Model will not depend on a specific mass transfer coefficient. However, the RTD of both, distributed and lumped approaches, can be approximated to each other by using the value k_{ds} of the latter as a fitting parameter for a given criterion of comparison. A plausible and convenient criterion is matching the second moment of both RTDs, as it is the lowest order moment affected by mass transport parameters of the stagnant zone.

The details for finding the fitting value of k_{ds} are given in Appendix A, where it is shown that k_{ds} is the same as that corresponding to the following analogous problem: a species (with

concentration $C \equiv Y$) is produced in the stagnant zone with uniform rate R at steady state, and is released to the dynamic region where its concentration is nil, *i.e.*:

$$\mathcal{D}_m \nabla^2 Y = -R, \quad \text{in } V_s; \qquad \nabla Y \cdot \mathbf{n} = 0, \quad \text{at } A_s; \qquad Y = 0, \text{ at } A_{ds} \quad (11)$$

Then, it follows that the matching coefficient k_{ds} is given by Eqs. (10a) and (10b) with $C_d = 0$ and $C \equiv Y$ satisfying system (11). By using the Gauss Theorem, it follows from Eqs. (10a), (10b) and (11):

$$k_{ds} = \frac{R}{A_{ds} \int_{V_s} Y \, dV} \quad (12)$$

As in problem (11) (Y/R) is independent of R, k_{ds} does not depend on R and, besides, the Sherwood number $Sh_{ds} = k_{ds} d_p / \mathcal{D}_m$ turns out to be also independent of d_p and $\mathcal{D}_m$ to become just a function of the angle φ (see inset in Fig. 1). The modified Sherwood number (Eq. (2)) can be written $Sh^* = Sh_{ds}(a_{ds} d_p)/(1-\varepsilon)$. Using (8) for a_{ds}:

$$Sh^* = 3 Sh_{ds} N_c \sin\varphi (1 - \cos\varphi) \quad (13)$$

System (11) was solved with COMSOL Multiphysics® software (numerical solution of differential equations by the finite elements method). The values of the volume V_s resulting from Eq. (5) with $\varepsilon = 0.4$, $N_c = 6$ and the range of H_s defined in Eq. (4), $0.01 < H_s < 0.06$, were considered. The corresponding values of the angle φ arise from Eq. (6). Values of Sh^* in the range $13 < Sh^* < 32$ thus result. This range covers the horizontal band indicated in Fig. 2, where, $Sh^*_{min} = 13$, $Sh^*_{max} = 32$. There is apparently no good reason to justify values of Sh^* lower than the lower limit $Sh^*_{min} = 13$, and the results in Fig. 2 below this limit can be regarded as being unreliable, in particular the data of Sicardi et al. [40] and Tamatsoulis and Papayannakos [42] correlation for powders.

As regards the high range of values of Sh^* in Fig. 2, we can appreciate that many data are well above the higher limit $Sh^*_{max} = 32$ for motionless stagnant regions, reaching up to more than two orders of magnitude higher. At this point we should call attention to the fact that all individual sets of data in Fig. 2 show a strong increase with Re_L, exception made of those of Bennet and Goodridge [25]. This consistent trend with Re_L along with the many data well above $Sh^*_{max} = 32$, strongly suggest that some part of the stagnant regions are stirred by the effect of the dynamic region. Although at the lower range of Re_L it may be particularly difficult to conceive a permanent convective cell inside the stagnant regions, the pulsing nature of the dynamic liquid flow may cause transient liquid recirculation inside them. Using a relationship of the form $Sh^* \propto Re_L^{\beta}$ for the individual data sets, this pulsing action may account for the high values arisen for the power β. For many sets, β is around 1 and rises up to around 2 for a few of them.

Therefore, it seems acceptable to find values of Sh^* higher than $Sh^*_{max} = 32$, but levels as higher as 2 orders of magnitude yet remain questionable. To explore further this feature, in first place we have considered for reference purposes the values of the global mass transfer coefficient k_{Lp}. We used the correlation of Rao and Drinkenburg [44], which was specifically developed from steady state mass transfer experiments between the liquid stream and the particle surface with prescribed concentration difference. For comparison with the data in Fig. 2, Rao and Drinkenburg's correlation was recast in the form,

$$Sh^*_{Lp} = \frac{a_{ds} k_{Lp} d_p^2}{(1-\varepsilon)\mathcal{D}_m} \quad (14)$$

where $a_{ds}/(1-\varepsilon)$ was estimated with the help of the geometrical model presented in Section 3, using the upper limit $H_s = 0.06$, which leads to the highest value of $a_{ds}/(1-\varepsilon)$ and, hence, of Sh^*_{Lp}. It should be kept in mind that k_{Lp} is an effective average of the relatively fast convective mass transfer process between the dynamic region and particles (through a_d) and the slower counterpart involving the serial steps dynamic region/stagnant region (through a_{ds}) and stagnant region/external particle surface (through a_s). The comparison was made under the expectation that Sh^*_{Lp} could compare at least in order of magnitude with Sh^*. However, Fig. 2 reveals that many experimental data of Sh^* surpass the Sh^*_{Lp} curve, reaching in some cases more than one order of magnitude in excess, at high values of Re_L.

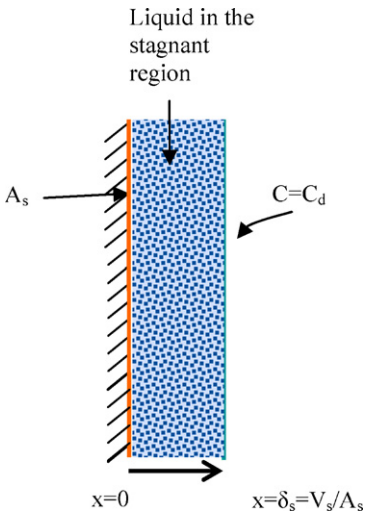

Fig. 4. Volume of stagnant region (V_s) uniformly distributed on the particle surface, A_s.

Such comparison may suggest a strong degree of unreliability of the highest values of Sh^*. Yet, it can be argued that the stagnant regions participate differently in the process characterized by Sh^*_{Lp} and that by Sh^*. In fact, for Sh^*_{Lp} the species is transferred all along the stagnant region up the particle surface, while Sh^* accounts (in the case of non-porous particles) for the filling and posterior depletion of the tracer within the stagnant liquid.

Therefore, an alternative upper estimation of Sh^* has been made by considering that the discussed effect of pulsing on the mass of the liquid inside the stagnant zone facilitates the access of the tracer into the inner areas adjacent to the particle surface, in particular those close to the contact point. As an extreme situation favorable to mass transport, we envisage that the volume of liquid in the stagnant region becomes uniformly distributed inside a motionless film confined by the particle surface (Fig. 4). The evaluation of Sh^* from this assumption is described in detail and further analyzed in Appendix B, where an upper estimation $Sh^* = 240$ is calculated. This estimation confirms, in a fully independent way, the impression gained from the comparison using Sh^*_{Lp} data points in Fig. 2 showing Sh^* larger than about 200 are highly unreliable.

Our conclusion is that values of Sh^* less than $Sh^*_{min} = 13$ and higher than about 200 can be hardly supported. Yet, the range $13 < Sh^* < 200$ spans one order of magnitude (Fig. 2).

4. Experimental results for coefficient k_{sp} and estimations from the Geometric Model

Values of the mass transfer coefficient k_{sp} between the stagnant regions and the subtended particle surface have been reported by Iliuta et al. [28] and Nigam et al. [29] by using tracer–response experiments with porous particles (see Tables 1 and 2). Essentially the same approach was employed in both contributions. Some parameters had to be evaluated from correlations (details given in the original references): k_{dp} (assumed equal to k_{Lp}), H_s (assumed equal to H_r), and the wetting efficiency f_w. The effective diffusivity $D_{eff} = (\varepsilon_p/\tau)\,\mathcal{D}_m$ inside the particles was taken from previous works

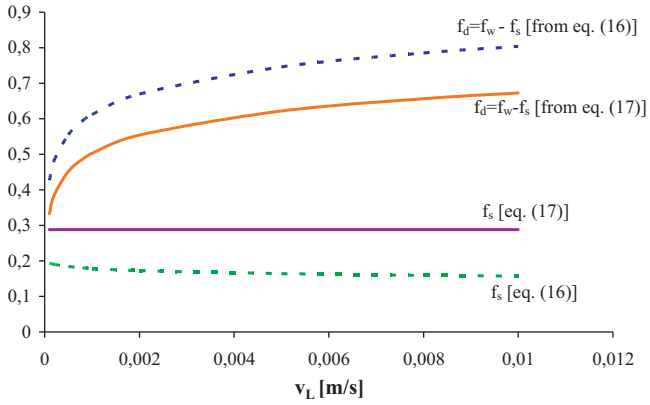

Fig. 5. Fraction of particle surface wetted by stagnant region, f_s, evaluated by Eqs. (16) and (17) and fraction of particle surface wetted by dynamic region, $f_d = f_w - f_s$.

from the authors. The fraction of particle surface wetted by dynamic (f_d) and stagnant regions (f_s) were estimated from the definition $f_s + f_d = f_w$ and the approximation proposed by Rajashekharam et al. [24],

$$\frac{f_d}{f_s} = \frac{H_d}{H_s} \tag{15}$$

As we have been employing specific surface areas, it is convenient to have in mind the relation between a fraction of particle surface f_i (i≡d,s,w) and the corresponding specific area: $a_i = 6f_i(1-\varepsilon)/d_p$. It is clear that the ratio between them is just an easily quantifiable coefficient.

As regards the treatment of transient diffusion inside the particles, Nigam et al. [29] employed a spherical geometry to approximate the behavior of non-spherical particles. Besides, in both works, Iliuta et al. [28] and Nigam et al. [29], spherical symmetry was assumed to solve the balances. This is a simplification even for spherical particles, as the different rates of mass transfer from the dynamic and stagnant zones break the symmetry.

The parameters for fitting model and experimental tracer-responses were the total hold-up, the axial dispersion coefficient D_L and the mass transfer parameters $a_{ds}k_{ds}$ and a_sk_{sp}.

It is evident that an important amount of predictions and assumptions likely to introduce some degree of uncertainty in the values of fitting parameters were employed. Although in general it becomes difficult to assess up to what extent the fitted parameters were affected, it is worth discussing in particular the use of approximation (15), as it concern directly the estimation of a_sk_{sp}.

From (15), $f_s + f_d = f_w$ and $H_t = H_d + H_s$

$$f_s = f_w \frac{H_s}{H_t} \tag{16}$$

The Geometric Model of Section 3 provides the relation (from Eqs. (8) and $a_s = 6f_s(1-\varepsilon)/d_p$):

$$f_s = \frac{1}{2}N_c(1-\cos\varphi) \tag{17}$$

In either cases, f_s from (16) or (17), $f_d = f_w - f_s$. The fractions f_s and f_d obtained from Eqs. (16) and (17) are plotted in Fig. 5, using as an example the correlations of Herskowitz [53] and Rao et al. [54] for f_w and H_t, respectively, and $H_s = 0.025$, $N_c = 6$. The case in Fig. 5 illustrates that the value of f_s (and hence of a_s) becomes significantly dependent on the assumption (15), which was proposed "as a first approximation" [24] and has no geometrical support. In general, the trend imposes by Eq. (15) is to over-predict f_d.

As in the data treatment of Iliuta et al. [28] and Nigam et al. [29], the product (f_dk_{dp}) accounting for the direct exchange between dynamic region and porous particles becomes determined beforehand, and probably overestimated, the contribution between the stagnant region and the porous particles (f_sk_{sp}), which was actually obtained from the regression procedure, was likely to be underestimated. The presumed low value used for f_s allows concluding that the value k_{sp} retrieved as $(f_sk_{sp})/f_s$ can be closer to the "true value" than the product (f_sk_{sp}). Hence, the data for the Biot number $Bi_{sp} = k_{sp}d_p/(2D_{eff})$, as reported by Iliuta et al. [28] and Nigam et al. [29] are plotted here in Fig. 6 and will be considered for further discussion.

Most results lie in the range $3 < Bi_{sp} < 12$. Some sets of data for the same particle show a very strong effect of Re_L. At variance with the coefficient k_{ds} discussed in Section 2.3.1, k_{sp} is a "conventional" mass transfer coefficient defined on the base of a true solid–fluid interface (A_s); hence, such strong variations with Re_L are likely to arise from the many assumptions undertaken and the simultaneous fitting of three parameters, rather than from a true effect of superficial liquid velocity. On the other hand, the authors report a negligible effect of the gas superficial velocity.

It is possible to carry out an analysis similar to that made in Appendix A to evaluate (by using the second moment of the simulated tracer-response experiments with porous particles) the relationship between the lumped description of the stagnant regions in the works of Iliuta et al. [28] and Nigam et al. [29] and the distributed description provided by the Geometric Model. However, only one global term coupling the distributed effects inside the particle and inside the elementary stagnant region is obtained

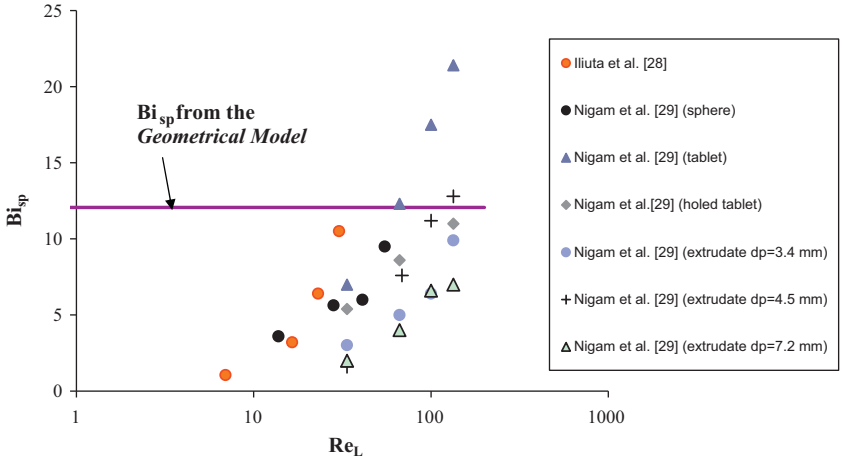

Fig. 6. Values of Biot number, $Bi_{sp} = k_{sp}d_p/(2D_{eff})$, reported by Iliuta et al. [28] and Nigam et al. [29], and from the Geometrical Model ($H_s = 0.01$, $D_{eff} = \mathcal{D}_m/2.93$).

when using the Geometric Model, from which one-to-one relations with the coefficients k_{dp}, k_{ds} and k_{sp} do not arise.

Given the complexity of the aforementioned approach, and recalling that the Geometric Model has been introduced to obtain lower estimates of the mass transfer rates, we have evaluated for comparison purposes the coefficient k_{sp} arisen from a steady state problem with prescribed uniform mass transfer flux j_{sp} on the elementary area A_s:

$$\mathcal{D}_m\nabla^2 C = 0, \quad \text{in } V_s; \qquad \mathcal{D}_m\nabla C\cdot\mathbf{n} = -j_{sp} \quad \text{at } A_s;$$
$$C = C_d, \quad \text{at } A_{ds} \tag{18a}$$

where j_{sp} and C_d are constants. The mass transfer coefficient k_{ds} and k_{sp} are defined as:

$$k_{ds}(C_d - C_s) = \frac{\mathcal{D}_m\int_{A_{ds}}(\nabla C\cdot\mathbf{n})dA}{A_{ds}} = j_{sp}\frac{A_s}{A_{ds}} \tag{18b}$$

$$k_{sp}(C_{sp} - C_s) = \frac{\mathcal{D}_m\int_{A_s}(\nabla C\cdot\mathbf{n})\,dA}{A_s} = -j_{sp} \tag{18c}$$

$$C_s = \frac{\int_{V_s} C\,dV}{V_s}; \qquad C_{sp} = \frac{\int_{A_s} C\,dA}{A_s} \tag{18d}$$

In (18a)–(18c), $\mathbf{n}$ is the unit vector normal to an element dA (of either A_s or A_{ds}) oriented outside the stagnant region. The second equalities in (18b) and (18c) arise from integrating the conservation equation in V_s and using the boundary condition at A_s (Eq. (18a)).

The prescribed flux at A_s leads to small mass transfer coefficients, as compared, *e.g.* with prescribed concentration, because of the geometry of the elementary stagnant region, that can be described as a cavity with small transversal areas for material access (maximum A_{ds}) and a large internal surface for material transfer (A_s). Therefore, the imposed flux j_{sp} at the inner regions close to the contact point makes an average large concentration difference (*i.e.* $C_{sp} - C_s$ in Eq. (18c)) to develop and low values of k_{sp} arise.

From solving (18a), the Sherwood numbers $Sh_{ds} = k_{ds}d_p/\mathcal{D}_m$ and $Sh_{sp} = k_{sp}d_p/\mathcal{D}_m$ were evaluated from (18b) and (18c) for the range of H_s defined in (4) and using $N_c = 6$.

From the range of Sh_{ds} values, $14 < Sh_{ds} < 23$, the resulting range of Sh^* (Eq. (13)) turns out to be $9 < Sh^* < 28.5$. We note that Sh^* values are not much lower than those obtained in Section 3.1 ($13 < Sh^* < 32$) from the analysis of non-porous particles.

As regards Sh_{sp}, a very narrow range arises: $8.2 < Sh_{sp} < 8.7$. From the lower limit (corresponding to $H_s = 0.01$), and using the relation $D_{eff} = \mathcal{D}_m/2.93$ (provided by Iliuta et al. [28]), a value $Bi_{sp} = k_{sp}d_p/(2D_{eff}) = 12$ is obtained, which has been indicated in Fig. 6 for comparison with the experimental data of Bi_{sp}.

The relevant conclusion from the comparison is that the k_{sp} values from the Geometric Model are not smaller than the experimental ones. The fact that for the most part the Geometric Model renders a larger value can be probably due to the assumptions made in the treatment of experimental data, as commented on above.

At this point, we recall again that the motivation for the present investigation is to find a reliable set of parameters to assess the effect of stagnant regions in TBRs. The resistance to mass transfer from the dynamic region to the particle surface subtended by the stagnant regions can be in this case described as that of a serial steady state process, from the dynamic region to the (bulk of the) stagnant regions, $(a_{ds}k_{ds})^{-1}$, followed by transfer from the stagnant region to the particle surface, $(a_sk_{sp})^{-1}$. In spite of the scatter of the experimental data, the analysis carried out in Section 2.3.1 points out that the former resistance is likely to be low (promoted by intermittent momentum transfer from the dynamic region). Thus, the available experimental information discussed in this section indicates that the inner resistance $(a_sk_{sp})^{-1}$ will be probably controlling, although its evaluation from experimental data is open to uncertainties. In this context, the Geometric Model can provide a valuable tool to predict consistent values of the controlling resistance $(a_sk_{sp})^{-1}$ that, as revealed by the comparison made in this section, are compatible with the experimental information. The Geometric Model can also provide a useful upper limit for the global resistance $\Omega_{dsp} = (a_sk_{sp})^{-1} + (a_{ds}k_{ds})^{-1}$, which roughly doubles the inner resistance. In this way, the effect of the stagnant regions on the performance of TBRs can be evaluated within reasonable tight bounds.

In this regards, it is interesting to evaluate the effect of the experimentally determined interval (4) for H_s. Expressing Ω_{dsp} as a global Sherwood number $Sh_{dsp} = d_p^2/(\Omega_{dsp}\mathcal{D}_m)$, the following range arises for the problem defined in (18a)–(18d):

$$2.7 < Sh_{dsp} < 6.8 \tag{19}$$

This range is narrower than that of H_s in (4) and its size may be regarded as satisfactory for the problem at hand.

A final important feature that additionally provides the use of the geometric Model is the possibility to evaluate the mass transfer rates under the proper boundary conditions on the particle surface, as arise when catalytic reactions are taken place inside the particles. As briefly discussed above, the geometry of the elementary stagnant region is such that the rate of mass transfer (*i.e.* as quantified by the coefficients k_{ds} and k_{sp}) are markedly affected by the magnitude of the rate of consumption/production of the species inside the catalytic particles.

The use of the Geometric Model to assess the behavior of TBRs is carried out at present and it is expected to report the results in a separate publication.

5. Conclusions

A critical revision has been carried out of experimental investigations, employing the tracer-response technique, to quantify the size of the liquid stagnant region in fixed beds with co-current gas-liquid down-flow, and its ability to exchange mass with the dynamic region and with the particles.

A very large dispersion of the volumetric coefficient $(a_{ds}k_{ds})$, accounting for exchange between the dynamic and stagnant regions, was the outstanding feature of the experimental data. Probably reasons for that spreading, including limitations of the experimental technique, modeling and regression procedures, were discussed. However, in our opinion, most relevant sources of uncertainty naturally arise because of two additional reasons. On one hand, the fluctuating nature of liquid flow in trickle beds makes uncertain the evaluation of fluid-dynamic and transport properties, in general. Secondly, the separation of the liquid into dynamic and stagnant regions is an artifact to simplify the complex behavior of the liquid flow interacting with strong forces exerted by the solid in the large areas around contact points between particles. This feature can be particularly relevant for the evaluation of the coefficient $(a_{ds}k_{ds})$, as there is no physically identifiable boundary between the two regions.

The second property analyzed was the hold-up H_s of the stagnant regions. Although considerable dispersion of the reported data was encountered, an interval within an order of magnitude could be identified (see range in 4).

The third property discussed in this contribution was the internal mass transfer coefficient k_{sp} between the stagnant regions and the subtended particle surfaces. This parameter was reported in only two contributions [28,29] employing porous particles. Even so, the degree of dispersion is important.

A model based on a geometrical characterization of an elementary stagnant region around the contact point (Geometric

Model) was proposed. The model just assumes molecular diffusion as the internal mechanism of mass transfer and thus its application is expected to provide lower estimations of the mass transfer processes involving the stagnant regions. In practice, the only significant parameter needed to define the model is the value of the stagnant liquid hold-up H_s.

This model was employed here as a reference to discuss the experimental data for the coefficients ($a_{ds}k_{ds}$) and k_{sp}. On one hand, many set of results showing very low values of ($a_{ds}k_{ds}$) could be assessed as being outside a "window of reliability". On the other hand, it became clear that a significant amount of data showing high values of ($a_{ds}k_{ds}$) can be accepted only by recognizing an important degree of liquid recirculation (of probably intermittent nature) inside the stagnant regions. In turn, the aspect ratio provided by the model ($d_p a_s/H_s$) allowed to estimate (Appendix B) a reasonable upper bound for values of ($a_{ds}k_{ds}$), which thus provides a further element to discriminate the experimental results.

The values of the inner coefficient k_{sp} estimated from the Geometric Model compares favorably, within an order of magnitude, with the experimental results [28,29].

The main motivation for the present investigation has been to identify a reliable set of parameters to assess the effect of stagnant regions in trickle bed reactors. The resistance to mass transfer from the dynamic region to the particle surface subtended by the stagnant regions corresponds in this case as that of a serial steady state process, from the dynamic region to the (bulk of the) stagnant regions, $(a_{ds}k_{ds})^{-1}$, followed by transfer from the stagnant region to the particle surface, $(a_s k_{sp})^{-1}$. The available experimental information discussed in this work indicates that the inner resistance $(a_s k_{sp})^{-1}$ will be probably controlling, although its evaluation is open to uncertainties. In this context, the Geometric Model can provide a valuable tool to predict consistent values of the controlling resistance $(a_s k_{sp})^{-1}$ that were shown to be compatible with the experimental information. The Geometric Model can also provide a useful upper limit for the global resistance $\Omega_{dsp} = (a_s k_{sp})^{-1} + (a_{ds}k_{ds})^{-1}$. In this way, the effect of the stagnant regions on the performance of trickle bed reactors could be evaluated within reasonable tight bounds.

Acknowledgment

The authors wish to thank the financial support of the following Argentine institutions: ANPCyT-SECyT (PICT N# 14/38336), CONICET (PIP N# 0304) and UNLP (PID N# 11/I136). O.M.M. and G.F.B. are Research Members of the CONICET.

Appendix A. Use of the Geometric Model to evaluate the coefficient ($a_{ds}k_{ds}$) arising in tracer-response experiments with non-porous particles

Here, we will evaluate the volumetric coefficient $a_{ds}k_{ds}$ as it would arise from the tracer-response experiments with non-porous particles when using the Geometric Model. It is assumed that the centered second moment is used as the fitting criterion to get $a_{ds}k_{ds}$ from the hypothetical tracer-response.

The transport of a tracer injected as a perfect pulse in the liquid feed of a trickle bed with non-porous particles is described by means of the following mass conservation balance in the dynamic region:

$$H_d \frac{\partial C_d}{\partial t} + \frac{\partial n}{\partial z} = -a_{ds} j_{ds} \tag{A1}$$

where n is the superficial molar flow of the tracer ($n = u_L C_d$ for the PE model and $n = u_L C_d - D_L\, \partial C_d/\partial z$ for the PDE model, Section 2.1) and j_{ds} is the local mass transfer flux from the dynamic to the stagnant regions. When the lumped description of the stagnant regions is used, $j_{ds} = k_{ds}(C_d - C_s)$ with k_{ds} uniform, while for the Geometric Model in Section 3 (distributed description), j_{ds} is given by the second equality in (10a).

We will assume here that only convective transport takes place in the sections upstream and downstream the bed. Thus, the response curve at the outlet of the bed ($z = Z$), $C_{d,Z}(t)$ is directly related to the RTD and its first moment $\bar{t}$ accounts for the mean residence time and the centered second moment accounts for the dispersion of the RTD:

$$\bar{t} = \frac{q_L}{M} \int_0^\infty C_{d,Z}(t)\, t\, dt \tag{A2}$$

$$\sigma^2 = \frac{q_L}{M} \int_0^\infty C_{d,Z}(t)\, t^2\, dt - \bar{t}^2 \tag{A3}$$

where q_L is the liquid flow rate and M the number of moles of tracer in the pulse injection.

We are interested here on the effect of the transport parameters of the stagnant regions on σ^2. To this end, it is convenient to work in Laplace transform domain. Thus, for any variable $y(t)$ depending on time t, its transform $\tilde{y}(p)$ is by definition

$$\tilde{y}(p) = \int_0^\infty y(t) e^{-pt}\, dt \tag{A4}$$

Any dependence of y with spatial coordinates is not made explicit in Eq. (A4). The following properties arise directly from definition (A4):

$$\tilde{y}^{(n)}(0) = (-1)^n \int_0^\infty y(t) t^n\, dt \tag{A5}$$

where

$$\tilde{y}^{(n)}(0) = \left. \frac{\partial^n \tilde{y}}{\partial p^n} \right|_{p=0} \tag{A6}$$

Then, Eqs. (A2) and (A3) can be rewritten,

$$\bar{t} = -\frac{q_L}{M} \tilde{C}^{(1)}_{d,Z}(0) \tag{A7}$$

$$\sigma^2 = \frac{q_L}{M} \tilde{C}^{(2)}_{d,Z}(0) - \bar{t}^2 \tag{A8}$$

To obtain expressions for $\tilde{C}^{(1)}_{d,Z}(0)$, $\tilde{C}^{(2)}_{d,Z}(0)$ we should transform first the balance (A1):

$$H_d[p\tilde{C}_d - C_{d0}] + \frac{\partial \tilde{n}}{\partial z} = -a_{ds}\tilde{j}_{ds} \tag{A9}$$

where C_{d0} is the tracer concentration just after the pulse injection (zero everywhere inside the bed, but at $z = 0$).

Evaluating (A9) and its first two derivatives respect to p at $p = 0$,

$$-H_d C_{d0} + \frac{\partial \tilde{n}(0)}{\partial z} = -a_{ds}\tilde{j}_{ds}(0) \tag{A10}$$

$$H_d \tilde{C}_d(0) + \frac{\partial\, \tilde{n}^{(1)}(0)}{\partial z} = -a_{ds}\tilde{j}^{(1)}_{ds}(0) \tag{A11}$$

$$2H_d \tilde{C}^{(1)}_d(0) + \frac{\partial\, \tilde{n}^{(2)}(0)}{\partial z} = -a_{ds}\tilde{j}^{(2)}_{ds}(0) \tag{A12}$$

Eqs. (A10)–(A12) can be solved (in z) sequentially, once closure expressions for $\tilde{j}_{ds}(0)$, $\tilde{j}^{(1)}_{ds}(0)$ and $\tilde{j}^{(2)}_{ds}(0)$ are obtained from the mass balances in the stagnant region. After that, $\bar{t}$ and σ^2 could be evaluated. As our purpose is to match the responses of the lumped description (Eq. (1)) and the Geometric Model (Eqs. (9a)–(9c)), under the criterion of obtaining the same value for the moments $\bar{t}$ and σ^2, it is not necessary to perform the whole solution, but it will suffice to match the expressions for $a_{ds}\tilde{j}_{ds}(0)$, $a_{ds}\tilde{j}^{(1)}_{ds}(0)$ and $a_{ds}\tilde{j}^{(2)}_{ds}(0)$ from the two approaches. This will guarantee the same value of $\bar{t}$

and σ^2. Hence, the next task is obtaining expressions for $a_{ds}\tilde{j}_{ds}(0)$, $a_{ds}\tilde{j}^{(1)}_{ds}(0)$ and $a_{ds}\tilde{j}^{(2)}_{ds}(0)$ according to both descriptions.

A.1. Closure for $\tilde{j}_{ds}(0)$, $\tilde{j}^{(1)}_{ds}(0)$ and $\tilde{j}^{(2)}_{ds}(0)$. Lumped description

The Laplace transform applied to Eq. (1) renders:

$$H_s(p\tilde{C}_s - C_{s0}) = a_{ds}k_{ds}(\tilde{C}_d - \tilde{C}_s) = a_{ds}\tilde{j}_{ds} \tag{A13}$$

where the tracer concentration C_{s0} after applying the injection pulse is zero at any z.

Evaluating (A13) and its first two derivatives respect to p at $p = 0$:

$$0 = a_{ds}k_{ds}[\tilde{C}_d(0) - \tilde{C}_s(0)] = a_{ds}\tilde{j}_{ds}(0) \tag{A14}$$

$$H_s\tilde{C}_s(0) = a_{ds}k_{ds}[\tilde{C}^{(1)}_d(0) - \tilde{C}^{(1)}_s(0)] = a_{ds}\tilde{j}^{(1)}_{ds}(0) \tag{A15}$$

$$2H_s\tilde{C}^{(1)}_s(0) = a_{ds}k_{ds}[\tilde{C}^{(2)}_d(0) - \tilde{C}^{(2)}_s(0)] = a_{ds}\tilde{j}^{(2)}_{ds}(0) \tag{A16}$$

Solving (A14) for $\tilde{C}_s(0)$ gives : $\tilde{C}_s(0) = \tilde{C}_d(0)$.

Solving (A15) for $\tilde{C}^{(1)}_s(0)$ gives : $\tilde{C}^{(1)}_s(0) = \tilde{C}^{(1)}_d(0) - \tilde{C}_d(0)[H_s/(a_{ds}k_{ds})]$

Solving (A16) for $\tilde{C}^{(2)}_s(0)$ gives : $\tilde{C}^{(2)}_s(0) = \tilde{C}^{(2)}_d(0) - 2H_s[(\tilde{C}^{(1)}_d(0)/a_{ds}k_{ds}) - (H_s\tilde{C}_d(0)/(a_{ds}k_{ds})^2)]$

The desired results are:

$$a_{ds}\tilde{j}_{ds}(0) = 0 \tag{A17}$$

$$a_{ds}\tilde{j}^{(1)}_{ds}(0) = \tilde{C}_d(0)H_s \tag{A18}$$

$$a_{ds}\tilde{j}^{(2)}_{ds}(0) = 2H_s\left[\tilde{C}^{(1)}_d(0) - \frac{H_s\tilde{C}_d(0)}{a_{ds}k_{ds}}\right] \tag{A19}$$

It is worth noting that only $\tilde{j}^{(2)}_{ds}(0)$ depends on k_{ds} and hence only $\tilde{C}^{(2)}_d(0)$ will depend on it. It follows from (A7) and (A8) that k_{ds} will affect σ^2, but not $\bar{t}$.

A.2. Closure for $\tilde{j}_{ds}(0)$, $\tilde{j}^{(1)}_{ds}(0)$ and $\tilde{j}^{(2)}_{ds}(0)$. Geometric Model

Applying the Laplace Transform to Eq. (9a)–(9c) and using $C_0 = 0$,

$$p\tilde{C} = \mathcal{D}_m\nabla^2\tilde{C}, \quad \text{in } V_s; \qquad \nabla\tilde{C}\cdot\mathbf{n} = 0, \quad \text{at } A_s;$$
$$\tilde{C} = \tilde{C}_d, \quad \text{at } A_{ds} \tag{A20a}$$

The transform flux $\tilde{j}_{ds}$ from Eq. (10a) is rewritten by means of the Gauss theorem and the no-flux condition at A_s in Eq. (A20a) as:

$$\tilde{j}_{ds} = \frac{\mathcal{D}_m\int_{V_s}\nabla^2\tilde{C}\,dV}{A_{ds}} \tag{A20b}$$

Evaluating (A20a) and (A20b) at $p = 0$

$$0 = \mathcal{D}_m\nabla^2\tilde{C}(0), \quad \text{in } V_s; \qquad \nabla\tilde{C}(0)\cdot\mathbf{n} = 0, \quad \text{at } A_s;$$
$$\tilde{C}(0) = \tilde{C}_d(0), \quad \text{at } A_{ds} \tag{A21a}$$

$$\tilde{j}_{ds}(0) = \frac{\mathcal{D}_m\int_{V_s}\nabla^2\tilde{C}(0)\,dV}{A_{ds}} \tag{A21b}$$

The solution for (A21a) is,

$$\tilde{C}(0) = \tilde{C}_d(0), \tag{A21c}$$

and from (A21b),

$$a_{ds}\tilde{j}_{ds}(0) = 0 \tag{A21d}$$

Differentiating (A20a) and (A20b) respect to p

$$\tilde{C} + p\tilde{C}^{(1)} = \mathcal{D}_m\nabla^2\tilde{C}^{(1)}, \quad \text{in } V_s; \qquad \nabla\tilde{C}^{(1)}\cdot\mathbf{n} = 0, \quad \text{at } A_s;$$
$$\tilde{C}^{(1)} = \tilde{C}^{(1)}_d, \quad \text{at } A_{ds} \tag{A22a}$$

$$\tilde{j}^{(1)}_{ds} = \frac{\mathcal{D}_m\int_{V_s}\nabla^2\tilde{C}^{(1)}\,dV}{A_{ds}} \tag{A22b}$$

Taking $p = 0$ in (A22a) and considering (A21c):

$$\tilde{C}_d(0) = \mathcal{D}_m\nabla^2\tilde{C}^{(1)}(0), \quad \text{in } V_s; \qquad \nabla\tilde{C}^{(1)}(0)\cdot\mathbf{n} = 0, \quad \text{at } A_s;$$
$$\tilde{C}^{(1)}(0) = \tilde{C}^{(1)}_d(0), \quad \text{at } A_{ds} \tag{A22c}$$

$$\tilde{j}^{(1)}_{ds}(0) = \frac{\mathcal{D}_m\int_{V_s}\nabla^2\tilde{C}^{(1)}(0)\,dV}{A_{ds}} \tag{A22d}$$

The system (A22c) should be solved numerically for $\tilde{C}^{(1)}(0)$, taking into account that $\tilde{C}_d(0)$ is constant in V_s. However, we find directly an expression for $\tilde{j}^{(1)}_{ds}(0)$, Eq. (A22d), by using the mass balance in V_s (A22c), and taking into account that $V_s/A_{ds} = H_s/a_{ds}$:

$$a_{ds}\tilde{j}^{(1)}_{ds}(0) = \tilde{C}_d(0)H_s \tag{A22e}$$

The final step is to find an expression for $\tilde{j}^{(2)}_{ds}(0)$. Differentiating (A22a) and (A22b) respect to p and fixing $p = 0$:

$$2\tilde{C}^{(1)}(0) = \mathcal{D}_m\nabla^2\tilde{C}^{(2)}(0), \quad \text{in } V_s;$$
$$\nabla\tilde{C}^{(2)}(0)\cdot\mathbf{n} = 0, \quad \text{at } A_s; \qquad \tilde{C}^{(2)}(0) = \tilde{C}^{(2)}_d(0), \quad \text{at } A_{ds} \tag{A23a}$$

$$\tilde{j}^{(2)}_{ds}(0) = \frac{\mathcal{D}_m\int_{V_s}\nabla^2\tilde{C}^{(2)}\,dV}{A_{ds}} \tag{A23b}$$

By using the mass balance in V_s (Eq. (A23a)) in (A23b), it is found for $a_{ds}\tilde{j}^{(2)}_{ds}(0)$:

$$a_{ds}\tilde{j}^{(2)}_{ds}(0) = a_{ds}\frac{2\int_{V_s}\tilde{C}^{(1)}(0)\,dV}{A_{ds}} \tag{A23c}$$

Now, for matching the lumped description to the Geometric Model, $a_{ds}\tilde{j}_{ds}(0)$, $a_{ds}\tilde{j}^{(1)}_{ds}(0)$ and $a_{ds}\tilde{j}^{(2)}_{ds}(0)$ from Eqs. (A17)–(A19) should match Eqs. (A21d), (A22e) and (A23c). The expression for $a_{ds}\tilde{j}_{ds}(0)$ and $a_{ds}\tilde{j}^{(1)}_{ds}(0)$ are identical, as far as the same value of H_s is taken for both descriptions, while for matching $a_{ds}\tilde{j}^{(2)}_{ds}(0)$ (equating (A19) and (A23c)), it is required that:

$$a_{ds}k_{ds} = -H_s\frac{\tilde{C}_d(0)}{(1/V_s)\int_{V_s}[\tilde{C}^{(1)}(0) - \tilde{C}^{(1)}_d(0)]\,dV} \tag{A24}$$

where we used again $V_s/A_{ds} = H_s/a_{ds}$.

In different words, if we assume that the Geometric Model is the true representation, but we employ the lumped description to interpret a tracer-response experiment using the criterion of the second centered moment σ^2, the value of $a_{ds}k_{ds}$ given in Eq. (A24) will be retrieved (provided that the correct model for the dynamic region is used and assuming ideal error-free experimental data).

Since the Geometric model depends for practical purposes only on H_s, the right hand side in (A24) can be calculated by solving first the problem (A22c). Problem (A22c) and Eq. (A24) can be recast in a more convenient way by introducing $Y \equiv \tilde{C}^{(1)}(0) - \tilde{C}^{(1)}_d(0)$, $R \equiv -\tilde{C}_d(0)$. It follows from (A22c):

$$-R = \mathcal{D}_m\nabla^2 Y, \quad \text{in } V_s; \qquad \nabla Y\cdot\mathbf{n} = 0, \quad \text{at } A_s; \qquad Y = 0, \quad \text{at } A_{ds} \tag{A25a}$$

The problem (A25a) corresponds to the steady state problem in the stagnant region with a uniform source rate R for a certain species of concentration Y, which is released to the dynamic region where

$Y = 0$. The mass transfer coefficient for (A25a) is given by the general definition (10a) in the main text:

$$k_{ds} Y_s = \frac{\mathcal{D}_m \int_{A_{ds}} (\nabla Y \cdot \mathbf{n})\, dA}{A_{ds}} \tag{A25b}$$

$$Y_s = \tfrac{1}{V_S} \int_{V_s} Y\, dV \tag{A25c}$$

Using the Gauss Theorem in (A25b), the balance in V_s from (A25a) and the ratio $V_s/A_{ds} = H_s/a_{ds}$, we obtain,

$$a_{ds} k_{ds} = -H_s \left(\frac{R}{Y_s} \right) \tag{A25d}$$

Then, the value of $a_{ds}k_{ds}$ from (A25d) is the same as that in (A24).

Appendix B. Upper estimation of the coefficient ($a_{ds}k_{ds}$) for a tracer experiment with non-nonporous particles

In this Appendix, an upper estimation of Sh^* will be made, based on the experimentally observed effect of Re_L on Sh^*. The effect of Re_L is interpreted by considering that pulsing of the liquid streamlines (dynamic region) causes an intermittently movement of the mass of liquid inside the stagnant zone. This movement allows the tracer to access more easily the inner areas adjacent to the particle surface, in particular those close to the contact point. As an extreme situation favorable to mass transport, we envisage that the volume of liquid in the stagnant region becomes uniformly distributed inside a motionless film confined by the particle surface. The other face of the film is bounded by the dynamic region.

Adopting the magnitudes quantified by the Geometric Model in Section 3, the half-volume V_s is thus reallocated over a plate of area A_s (see inset in Fig. 1) and thickness δ_s, such that $V_s = A_s\delta_s$, as illustrated in Fig. 4. The following expressions quantify the tracer exchange between an elementary stagnant region thus conceived and the dynamic region (see Fig. 4) during a tracer-response experiment with non-porous particles:

$$\frac{\partial C}{\partial t} = \frac{\mathcal{D}_m \partial^2 C}{\partial z^2}, \quad \text{in } 0 < z < \delta_s; \qquad \frac{dC}{dz} = 0, \quad \text{at } z = 0;$$
$$C = C_d, \quad \text{at } z = \delta_s \tag{B1a}$$

$$j_{ds} = \mathcal{D}_m \left. \frac{\partial C}{\partial z} \right|_{z=\delta_s} \tag{B1b}$$

By following completely similar lines as those in Appendix A when the RTD moments are employed to estimate the model parameters, the coefficient k_{ds} arises from solving the following steady state problem:

$$-R = \mathcal{D}_m \frac{d^2 Y}{dz^2}, \quad \text{in } 0 < z < \delta_s; \qquad \frac{dY}{dz} = 0, \quad \text{at } z = 0;$$
$$Y = 0, \quad \text{at } z = \delta_s \tag{B2a}$$

Then,

$$k_{ds} = \frac{R\delta_s^2}{\int_0^{\delta_s} Y\, dz} \tag{B2b}$$

Solving (B2a) produces the profile $Y = (\delta_s^2 - z^2)R/(2\mathcal{D}_m))$ and from (B2b)

$$k_{ds} = \frac{3\mathcal{D}_m}{\delta_s} \tag{B3}$$

Replacing $\delta_s = V_s/A_s$ and noting that according to the present description the specific area of the boundary between the stagnant and dynamic zones is $a_{ds} \equiv a_s$, we obtained for Sh^*

$$Sh^* = \frac{3a_s d_p^2 A_s}{(1-\varepsilon)V_s} \tag{B4}$$

Using Eqs. (6)–(8) for V_s, A_s and a_s, according to the Geometric Model:

$$Sh^* = \frac{108\, N_c}{(1 + 2\cos\varphi)} \tag{B5}$$

where it is recalled that φ arises by combining Eqs. (5) and (6). Using the upper limit $H_s = 0.06$, along with $\varepsilon = 0.4$, $N_c = 6$, renders the highest value of Sh^*, which thus becomes $Sh^* = 240$.

It is important to note that with this set of parameters, $\delta_s = V_s/A_s = d_p/28$. To illustrate that this value leads to an upper estimation of Sh^*, we can compare it with the effective thickness arisen from the mass transfer coefficient between the bulk of the stagnant region and the particle surface, k_{sp}, discussed in Section 4. The highest experimental value of $Bi_{sp} = k_{sp}d_p/(2D_{eff})$ reported in Fig. 6 is about $Bi_{sp} = 22$. In those experiments $D_{eff} = \mathcal{D}_m/2.93$. It follows that $Sh_{sp} = k_{sp}d_p/\mathcal{D}_m = 15$ which according to the film theory corresponds to an effective thickness $\delta_{sp} = d_p/Sh_{sp} = d_p/15$. As δ_{sp} is the thickness of a film inside the stagnant region, it can be expected to be lower than δ_s, which represents the thickness of the whole region. The opposite result ($\delta_{sp} \approx 2\delta_s$) is an evidence that δ_s is a lower estimation and $Sh^* = 240$ an upper estimation.

References

[1] O.M. Martínez, M.C. Casanello, A.L. Cukierman, Three-phase fixed bed catalytic reactors: application to hydrotreatment processes, Trends Chem. Eng. 2 (1994) 393–453.
[2] E. Furimsky, Selection of catalysts and reactors for hydroprocessing, Appl. Catal. 171 (1998) 177–206.
[3] G. Biardi, G. Baldi, Three-phase catalytic reactors, Catal. Today 52 (1999) 223–234.
[4] S.P. Bressa, N.O. Ardiaca, O.M. Martínez, G.F. Barreto, Analysis of operating variables in the catalitic purification of 1-butane in a trickle-bed, Chin. J. Chem. Eng. 6 (1998) 103–115.
[5] K. Kiared, A. Zoulalian, Study and modelling of catalytic sulfur dioxide oxidation in verlifix three-phase reactor, Chem. Eng. Sci. 47 (1992) 3705–3712.
[6] S.T. Sie, R. Krishna, Fundamentals and selection of advanced Fischer–Tropsh reactors, Appl. Catal. 186 (1999) 55–70.
[7] M.P. Dudukovic, F. Larachi, P.L. Mills, Multiphase reactors—revisited, Chem. Eng. Sci. 54 (1999) 1975–1995.
[8] F.L. Smith, G.A. Sorial, M.T. Suidan, A. Pandit, P. Biswas, R.C. Brenner, Evaluation of trickle bed air biofilter performance as a function of inlet VOC concentration and loading, and biomasss control, J. Air Waste Manage. Assoc. 48 (1998) 627–636.
[9] A. Fortuny, C. Bengoa, J. Font, F. Castells, A. Fabregat, Water pollution abatement by catalytic wet air oxidation in a trickle bed reactor, Catal. Today 53 (1999) 107–114.
[10] G.I. Horowitz, O.M. Martínez, A.L. Cukierman, M.C. Cassanello, Effect of the catalyst wettability on the performance of a trickle-bed reactor for ethanol oxidation as a case study, Chem. Eng. Sci. 54 (1999) 4811–4816.
[11] F.S. Mederos, J. Ancheyta, J. Chen, Review on criteria to ensure ideal behaviors in trickle-bed reactors, Appl. Catal. A 355 (2009) 1–19.
[12] M.H. Al-Dahhan, F. Larachi, M.P. Dudukovic, A. Laurent, High-pressure trickle-bed reactors: a review, Ind. Eng. Chem. Res. 36 (1997) 3292–3314.
[13] A.K. Saroha, K.D.P. Nigam, Trickle bed reactors, Rev. Chem. Eng. 12 (1996) 207–347.
[14] A. Gianetto, V. Specchia, Trickle-bed reactors: state of art and perspectives, Chem. Eng. Sci. 47 (1992) 3197–3213.
[15] T.B. Zhukova, V.N. Pisarenko, V.V. Kafarov, Modeling and design of industrial reactors with a stationary bed of catalyst and two-phase gas-liquid flow—a review, Int. Chem. Eng. 30 (1990) 57–102.
[16] A. van Houwelingen, The morphology of solid-liquid contacting efficiency in trickle flow, Master Dissertation, University of Pretoria, Republic of South Africa, 2006.
[17] P.V. Ravindra, D.P. Rao, M.S. Rao, Liquid flow texture in trickle-bed reactors: an experimental study, Ind. Chem. Eng. Res. 36 (1997) 5133–5145.
[18] M.H. Sankey, D.J. Holland, A.J. Sederman, L.F. Gladden, Magnetic resonance velocity imaging of liquid and gas two-phase flow in packed beds, J. Magn. Reson. 192 (2009) 142–148.

[19] G. Liu, Z. Mi, L. Wang, X. Zhang, S. Zhang, Hydrogenation of dicyclopentadiene into endo-tetrahydrodyciclopentadiene in trickle-bed reactor: experiments and modelling, Ind. Eng. Chem. Res. 45 (2006) 8807–8814.
[20] T.A. Nijhuis, F.M. Dautzenberg, J.A. Moulijn, Modeling of monolithic and trickle-bed reactors for the hydrogenation of styrene, Chem. Eng. Sci. 58 (2003) 1113–1124.
[21] A. Eftaxias, F. Larachi, F. Stüber, Modelling of trickle bed reactor for the catalytic wet air oxidation of phenol, Can. J. Chem. Eng. 81 (2003) 784–794.
[22] R.V. Chaudhari, R. Jaganathan, S.P. Mathew, C. Julcour, H. Delmas, Hydrogenation of 1,5,9-cyclododecatriene in fixed-bed reactors: down- vs upflow modes, AIChE J. 48 (2002) 111–125.
[23] I. Iliuta, F. Larachi, Wet air oxidation solid catalysis analysis of fixed and sparged three-phase reactors, Chem. Eng. Process. 40 (2001) 175–185.
[24] M.V. Rajashekharam, R. Jaganathan, R.V. Chaudhari, A trickle-bed reactor model for hydrogenation of 2,4 dinitroluene: experimental verification, Chem. Eng. Sci. 53 (1998) 787–805.
[25] A. Bennett, F. Goodridge, Hydrodynamic and mass transfer studies in packed absorption columns. Part I. Axial liquid dispersion, Trans. Inst. Chem. Eng. 48 (1970) T232–T240.
[26] G.J. Hoogendoorn, J. Lips, Axial mixing of liquid in gas-liquid flow through packed beds, Can. J. Chem. Eng. 43 (1965) 125–131.
[27] I. Iliuta, F.C. Thyrion, O. Muntean, Residence time distribution of the liquid in two-phase cocurrent downflow in packed beds: air/newtonian and non-newtonian liquids systems, Can. J. Chem. Eng. 74 (1996) 783–796.
[28] I. Iliuta, F. Larachi, B.P.A. Grandjean, Residence time, mass transfer and back-mixing of the trickle flow reactors containing porous particles, Chem. Eng. Sci. 54 (1999) 4099–4109.
[29] K.D.P. Nigam, I. Iliuta, F. Larachi, Liquid back-mixing and mass transfer effects in trickle-bed reactors filled with porous catalyst particles, Chem. Eng. Process. 41 (2002) 365–371.
[30] X.L. Yang, J.P. Euzen, G. Wild, Residence time distribution of the liquid in gas–liquid cocurrent upflow fixed-bed reactors with porous particles, Chem. Eng. Sci. 45 (1990) 3311–3317.
[31] I. Iliuta, F.C. Thyrion, O. Muntean, Hydrodynamic characteristics of two-phase flow through fixed beds: air/newtonian and non-newtonian liquids, Chem. Eng. Sci. 51 (1996) 4987–4995.
[32] C. Julcour-Lebigue, L. Baussaron, H. Delmas, A.M. Wilhelm, Theoretical analysis of tracer method for the measurement of wetting efficiency, Chem. Eng. Sci. 62 (2007) 5374–5379.
[33] D.M. Himmelblau, K.B. Bischoff, Process Analysis and Simulation, Wiley, New York, 1968.
[34] A. Matsuura, T. Akehata, T. Shirai, Axial dispersion of liquid in concurrent gas–liquid downflow in packed beds, J. Chem. Eng. Jpn. 9 (1976) 294–301.
[35] W.P.M. Van Swaaij, J.C. Charpentier, J. Villermaux, Residence time distribution in the liquid phase of trickle flow in packed columns, Chem. Eng. Sci. 24 (1969) 1083–1095.
[36] J. Villermaux, W.P.M. Van Swaaij, Modèle representatif de la distribution des temps de sèjour dans un réacteur semi-infini à dispersión axiale avec zones stagnantes. Application à l'écoulement ruisselant dans des colonnes d'anneaux Raschig, Chem. Eng. Sci. 24 (1969) 1097–1111.
[37] F. De Maria, R.R. White, Transient response study of gas flowing through irrigated packing, AIChE J. 6 (1960) 473–481.
[38] R. Joubert, W. Nicol, Multiplicity behavior of trickle flow liquid–solid mass transfer, Ind. Eng. Chem. Res. 48 (2009) 8387–8392.
[39] K.B. Bischoff, E.A. McCracken, Tracer test in flow systems, Ind. Eng. Chem. 58 (1966) 18–31.
[40] S. Sicardi, G. Baldi, V. Specchia, Hydrodynamic models for the interpretation of the liquid flow in trickle-bed reactors, Chem. Eng. Sci. 35 (1980) 1775–1782.
[41] J.M. Hochman, E. Effron, Two-phase cocurrent downflow in packed beds, Ind. Eng. Chem. Fundam. 8 (1969) 63–71.
[42] D. Tsamatsoulis, N. Papayannakos, Simulation of no-ideal flow in a trickle bed hydrotreater by the cross-flow model, Chem. Eng. Sci. 50 (1995) 3685–3691.
[43] A.E. Saez, R.G. Carbonell, Hydrodynamic parameters for gas-liquid cocurrent flow in packed beds, AIChE J. 31 (1985) 52–62.
[44] V.G. Rao, A.A.H. Drinkenburg, Solid–liquid mass transfer in packed beds with cocurrent gas–liquid downflow, AIChE J. 31 (1985) 1059–1068.
[45] W. van der Merwe, C. Maree, W. Nicol, Nature of residual liquid holdup in packed beds of spherical particles, Ind. Eng. Chem. Res. 43 (2004) 8363–8368.
[46] D. Stegeman, F.E. van Rooijen, A. Kamperman, S. Weijer, K.R. Westerterp, Residence time distribution in the liquid phase in a cocurrent gas–liquid trickle-bed reactor, Ind. Eng. Chem. Res. 35 (1996) 378–385.
[47] C.N. Schubert, R.M. Lindner, R.M. Kelly, Experimental methods for measuring static liquid holdup in packed columns, AIChE J. 32 (1986) 1920–1923.
[48] S. Sicardi, G. Baldi, A. Gianetto, V. Specchia, Catalyst areas wetted by flowing and semistagnant liquid in trickle-bed reactors, Chem. Eng. Sci. 35 (1980) 67–73.
[49] A. Ortiz-Arroyo, F. Larachi, I. Iliuta, Method for inferring contact angle and for correlating static liquid hold-up in packed beds, Chem. Eng. Sci. 58 (2003) 2835–2855.
[50] Z.S. Mao, T.Y. Xiong, J.Y. Chen, Theorical prediction of static liquid hold-up in trickle bed reactors and comparison with experimental results, Chem. Eng. Sci. 48 (1993) 2697–2703.
[51] J. Reimann, R.A. Pieritz, C. Ferrero, M. di Michiel, R. Rolli, X-ray tomography investigations on pebble bed structures, Fusion Eng. Des. 83 (2008) 1326–1330.
[52] W.I. Salvat, N.J. Mariani, O.M. Martínez, G.F. Barreto, Propiedades de contacto en lechos rellenos de esferas monodispersas en recipientes cilíndricos, in: Actas del XIV Congreso Argentino de Catálisis, 622-627, XIV Congreso Argentino de Catálisis, Santa Fe, Argentina, 2005.
[53] M. Herskowitz, Wetting efficiency in trickle-bed reactors—its effect on the reactor performance, Chem. Eng. J. Biochem. Eng. J. 22 (1981) 167–175.
[54] V.G. Rao, M.S. Ananth, Y.B.G. Varma, Hydrodynamics of two-phase cocurrent downflow through packed beds. II. Experimental and correlations, AIChE J. 29 (1983) 473–483.